Applied Catalysis B: Environmental 140–141 (2013) 9–15

Contents lists available at SciVerse ScienceDirect

Applied Catalysis B: Environmental

journal homepage: www.elsevier.com/locate/apcatb

Low-temperature synthesis and characterization of rutile nanoparticles with amorphous surface layer for photocatalytic degradation of caffeine

Matic Krivec[a,c,*], Ricardo A. Segundo[b], Joaquim L. Faria[b], Adrián M.T. Silva[b], Goran Dražić[a,c]

[a] Jožef Stefan Institute, Department for Nanostructured Materials, Jamova cesta 39, SI-1000 Ljubljana, Slovenia
[b] LCM – Laboratory of Catalysis and Materials – Associate Laboratory LSRE/LCM, Faculdade de Engenharia, Universidade do Porto, Rua Dr. Roberto Frias, 4200-465 Porto, Portugal
[c] Jožef Stefan International Postgraduate School, Jamova cesta 39, SI-1000 Ljubljana, Slovenia

ARTICLE INFO

Article history:
Received 4 January 2013
Received in revised form 11 March 2013
Accepted 27 March 2013
Available online 4 April 2013

Keywords:
Rutile nanoparticles
Low-temperature hydrothermal synthesis
Amorphous surface layer
Photocatalysis

ABSTRACT

Rutile (TiO_2) nanoparticles were prepared by a low-temperature hydrothermal process from titanium(IV) isopropoxide as a precursor and without any additional calcination step. The particles were characterized with several techniques (XRD, BET, UV–vis spectrometry, TEM/HRTEM/SAED, FT-IR) and their photocatalytic efficiency was evaluated on the degradation of caffeine. The as-prepared rutile particles exhibited a rod-like morphology with a prism body and pyramidal ends. The low-temperature hydrothermal synthesis introduced an amorphous layer that was around 1-nm thick and uniformly covered the surfaces of the particles. The enhanced photocatalytic properties of the particles confirmed the positive impact of the amorphous surface layer in comparison to the fully crystallized surface of commercial rutile particles and to particles that were synthesized using a conventional high-temperature calcination route. The amorphous surface layer seems to enhance the adsorption of both oxygen and caffeine on the surface of the particles and, therefore, improves the photocatalytic activity of the rutile particles. Being the case, the electron transfer to the adsorbed oxygen is more efficient, increasing the life-time of the photogenerated holes, which contributes to the degradation of caffeine via the formation of reactive radicals and/or by direct oxidation.

1. Introduction

In recent years, the remediation of hazardous wastes, contaminated groundwaters and toxic air has attracted the attention of scientists all over the world. In order to overcome this problem, extensive research is being conducted to develop new methods for the characterization and elimination of hazardous chemicals from air, soil and water [1].

Semiconductor photocatalysis is a physicochemical method that exploits the characteristic electronic structure of the material and is able to directly or indirectly enhance the oxidation of different pollutants [1].

TiO_2 is known to be the most promising material for semiconductor photocatalysis, not only because of its adequate band-gap energy and thermodynamics of the valence and conduction bands, but also because of the chemical properties of the surface, which play a major role in the photocatalytic process [2].

Photocatalysis has been extensively investigated on two crystal modifications of TiO_2: anatase and rutile. Rutile has shown much lower photocatalytic activity than anatase in all types of reaction media and in the presence of oxygen gas [2]. There are various properties that can explain the superiority of anatase over the rutile phase in terms of photocatalysis. The first one is the electron–hole recombination: rutile has a smaller band-gap than anatase, which means that excited electrons recombine with photogenerated holes faster and, therefore, do not participate in the photocatalytic reaction [3]. The second one is the hydroxylation degree of the adsorbed surface: rutile is normally obtained at high temperatures, which induces irreversible dehydroxylation of the surface and reduces the photocatalytic properties [2,4], while the surface of anatase is commonly highly hydroxylated and, therefore, oxygen and water molecules can adsorb on its surface and initiate the photocatalytic reaction. The next important feature is the particle size: smaller particles have higher specific surface areas. Rutile is thermodynamically the most stable crystalline form at all temperatures and is particularly stable for particles larger than 35 nm, while for

* Corresponding author at: Jožef Stefan Institute, Department for Nanostructured Materials, Jamova cesta 39, SI-1000 Ljubljana, Slovenia. Tel.: +386 1 4773 821; fax: +386 1 4773 221.
E-mail address: matic.krivec@ijs.si (M. Krivec).

0926-3373/$ – see front matter © 2013 Elsevier B.V. All rights reserved.
http://dx.doi.org/10.1016/j.apcatb.2013.03.045

particles smaller than 11 nm the metastable anatase form dominates; therefore, the size alone provides a good explanation for the better photocatalytic activity of the anatase phase [5]. The reality, however, is not so straightforward: smaller particles usually have a lower crystallinity and therefore a larger number of defects that enhance the recombination of the electron/hole pairs. Furthermore, below a certain size there is an inversion on the band gap energy, increasing it, which lowers their photocatalytic activity [5–7].

On the basis of the described the rutile phase has been regarded as the less-favorable modification of TiO_2 in terms of photocatalytic activity. Nevertheless, rutile particles have an advantage in terms of their activation energy: the smaller band-gap (3.0 eV) of the material enables the use of visible-light illumination, which can be a major factor in the synthesis of photocatalytic materials. The traditional preparation method for rutile particles is the high-temperature calcination of anatase particles that transforms the anatase to rutile above 600 °C [8]. This calcination treatment greatly affects the surface and the size of the particles; therefore, a low-temperature synthesis would be a reasonable solution in order to obtain improved photocatalytic properties for the rutile particles.

In this work the rutile particles were prepared on a two-step synthetic procedure: the first step was the well-established formation of a peroxotitanium complex between hydrogen peroxide molecules and Ti^{4+} ions [9]. The procedure was additionally upgraded with a hydrothermal treatment, in a second step. Both procedures were conducted at low-temperatures and the particles were not thermally treated at the end of the synthesis. The photocatalytic activity of the prepared samples was evaluated on the degradation of caffeine. This compound was chosen as a model degradation molecule for different reasons: it is the origin of domestic sanitary contamination and the mechanism of its degradation has been already investigated in an aqueous suspension of TiO_2 particles [10,11]. The structural and photocatalytical properties of the as-prepared particles were compared with two commercial rutile particles and also with rutile particles synthesized using the traditional high-temperature method. The influence of the structure of the surface on the photocatalytic efficiency is discussed and explained.

2. Materials and methods

2.1. Chemicals

Titanium(IV) isopropoxide (TIP: $Ti(OCH(CH_3)_2)_4$, Acros Organics, New Jersey, USA), hydrogen peroxide (H_2O_2, 35 wt.%, Acros Organics, New Jersey, USA), isopropanol ($CH_3CH(OH)CH_3$, AppliChem GmbH, Darmstadt, Germany), nitric acid (HNO_3, 65%, AppliChem GmbH, Darmstadt, Germany) and caffeine (≥99.0% HPLC grade, Sigma–Aldrich Chemie GmbH, Steinheim, Germany) were used without further purification.

2.2. Samples preparation

TiO_2 nanoparticles were prepared in a two-step synthesis procedure. In the first step, TIP diluted with isopropanol was added dropwise to an aqueous solution of H_2O_2 under vigorous stirring. A molar ratio [H_2O_2]: [Ti] of 20 was used for a Ti concentration of 0.158 M at pH of 0.5 adjusted with HNO_3, according to Zhang et al. [9]. The red solution was cooled with ice until the particles started to precipitate. The resulting orange suspension was further treated at 70 °C under reflux conditions for 24 h.

In the second step (hydrothermal treatment), 50 mL of reflux suspension was put inside a Teflon-lined stainless-steel autoclave (50% filling). The autoclave was placed inside a heating chamber with mechanical convection (Binder FED 53) and set to 75 °C for 8, 24 and 96 h (HT8, HT24, HT96). The precipitate was washed with de-ionized water three times and dried at room temperature.

As-prepared samples were compared with three rutile powders: commercial rutile Tronox (C1, Tronox Incorporated, Oklahoma City, USA), rutile particles from Cinkarna Celje (C2, Cinkarna Celje d.d., Celje, Slovenia) and a third sample prepared with the sol–gel synthesis of the anatase phase from a TIP precursor and the traditional conversion to the rutile phase at 800 °C (T800).

2.3. Materials characterization

The phases in the samples were characterized by powder X-ray diffraction (XRD) using a PANalytical X'Pert PRO diffractometer.

The specific surface area measurements (BET) were conducted using a Micromeritics Gemini II 2370 Surface Area Analyzer.

An FT-IR spectrophotometer (PerkinElmer Spectrum 100 FT-IR) equipped with TGS detector and an ATR (attenuated total reflection) module was used for the surface characterization of the TiO_2 particles. The TiO_2 powder was pressed on the ATR window (d = 2 mm) and the spectra were collected from 4 scans, each with a nominal resolution of 2 cm^{-1}. The background was measured with the ATR module without any sample.

The diffuse-reflectance UV–vis spectra of the photocatalysts were measured on a JASCO V-560 UV-Vis spectrophotometer equipped with an integrating sphere (JASCO ISV-469). $BaSO_4$ powder was used as a reference to provide a 100% reflectance measurement. The spectra were recorded in the diffuse reflectance mode and transformed by the instrument software (JASCO) to equivalent absorption Kubelka–Munk units and then the band-gap values were determined.

The particles were investigated with a JEOL 2010F transmission electron microscope equipped with a field emission gun. The microscope was operated at 200 kV.

2.4. Photocatalytic experiments

The photocatalytic activities of the TiO_2 powder samples were investigated by measuring the degradation of a 50 mg L^{-1} caffeine solution under UV/vis illumination source (Heraeus TQ 150 medium-pressure mercury-vapor lamp), in a setup described elsewhere [12]. A DURAN® glass cooling jacket was used to obtain irradiation in the near-UV to visible light range (λ > 350 nm; main emission lines at 366, 436 and 546 nm). The photon flow entering the reactor was determined with an Ocean Optics spectroradiometer positioned in the photoreactor, i.e. 4 cm away from the lamp, the total irradiance at this point being equal to 27 mW cm^{-2}. In a typical experiment, 7.5 mg of a TiO_2 sample was mixed with 7.5 mL of the caffeine aqueous solution inside a 10-mL quartz reactor. The reaction was performed in the presence of oxygen or argon flow as well as under natural dissolved oxygen, separately. The suspension was firstly stirred for 30 min in the dark to achieve the absorption–desorption equilibrium of caffeine on the surface of the particles. Afterwards, the reactor was exposed to the illumination source (t = 0 min for reaction) and samples were taken from it during different periods of the reaction. The concentration of caffeine was monitored by a high-performance liquid chromatography apparatus (Hitachi Elite LaChrom) equipped with a diode array detector (L-2450) and a solvent delivery pump (L-2130). A gradient method at a constant flow rate of 1 mL min^{-1} was used in a Purospher Star RP-18 column (250 mm × 4.6 mm; 5 μm particles). First, the column was equilibrated with a A:B (70:30) mixture of milli-Q water (A) and methanol (B), followed by a linear gradient run to A:B (20:80) in 30 min and finally with isocratic elution over a period of 2 min.

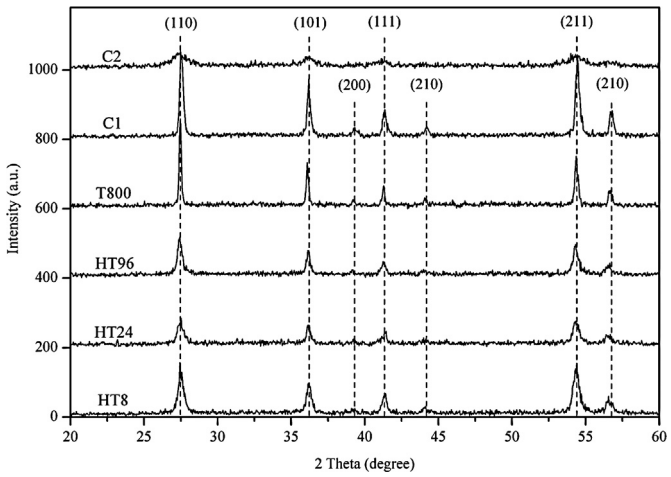

Fig. 1. XRD patterns of rutile TiO_2 samples synthesized for different times of the hydrothermal treatment: HT8, HT24, HT96; rutile particles synthesized by a standard high-temperature technique: T800; and two commercial rutile samples: C1 and C2.

3. Results and discussion

3.1. XRD and BET analysis

The XRD patterns of the synthesized and commercial TiO_2 particles are shown in Fig. 1.

The particles prepared using the low-temperature hydrothermal technique (HT8, HT24, HT96) have four intense diffraction peaks at $2\theta = 27.3^\circ$, 35.9°, 41.2°, 54.4° and three minor peaks at $2\theta = 39.2^\circ$, 43.7°, 56.5°, corresponding to the (1 1 0), (1 0 1), (1 1 1) and (2 1 1) along with the (2 0 0), (2 1 0) and (2 2 0) crystal planes of the rutile TiO_2 phase, respectively [13–15]. The relative intensities of the peaks are similar between all the samples and, therefore, it is difficult to distinguish more or less crystalline materials. The diffraction peaks of the commercial samples (C1, C2) and the sample prepared by the phase-conversion process (T800) are at the same positions as in the other samples. The peaks of C1 and T800 are narrower than the peaks of the other samples, reflecting the different crystallite size. Broad peaks are seen in the case of the second commercial TiO_2 (C2). The signal-to-noise ratio indicates the presence of some amorphous phase, while the positions of the peaks suggest the presence of a pure rutile phase.

The average crystallite size (Table 1) was determined by the conventional Scherrer's method with the consideration of the full-width at half-maximum for the (1 1 0) peak. Considering the estimated experimental errors, the particles prepared with the low-temperature hydrothermal synthesis have around the same crystallite size (13–14 nm). Therefore, longer time of the hydrothermal synthesis has negligible impact on the crystallite size. The sample prepared at high temperature has a significant larger crystallite size of 50 nm. The estimated crystallite sizes of the commercial rutile samples are 28 nm (C1) and 8 nm (C2).

The specific surface area can affect the catalytic behavior of a photocatalyst. The determined specific BET surface areas are shown in Table 1. The highest specific surface area was measured in the case of the commercial C2 sample ($164\ m^2\ g^{-1}$). The specific surface areas of the low-temperature prepared samples were similar ($62–65\ m^2\ g^{-1}$) and lower than $10\ m^2\ g^{-1}$ for C1 and T800.

The band-gap measurements (not-shown) confirmed the rutile phase of the TiO_2 particles (around 3.0 eV, as shown in Table 1). The band-gap values of the hydrothermally treated, C1 and C2 samples are a little higher than expected, which can be attributed to the impact of the quantum size effect [16]. On the other hand, the measured band-gap of T800 sample was not affected by the quantum size effect, probably due to its larger particle size, the obtained value being the closest to the predicted band-gap of rutile (3.0 eV).

3.2. Surface characterization

3.2.1. TEM analysis

Fig. 2 shows micrographs obtained by the transmission electron microscopy (TEM), some with high resolution (HRTEM), for the commercial rutile particles (a,b) and the rutile particles prepared with the high-temperature calcination (c).

The particles from the commercial C1 sample (Fig. 2a) and the T800 sample (Fig. 2c) are large and highly agglomerated. The surfaces of these particles are mostly crystalline and clean, as seen in the insets of each picture. The second commercial sample (C2) has particles with a more elongated morphology and uniform size (Fig. 2b). Observing the electron diffraction pattern, small rutile particles are identified (from slightly diffuse uniform circles). Still, amorphous phase could not be excluded. In the HRTEM micrograph is visible that the particles surface is coated by a small portion of amorphous phase. Low-temperature synthesis produces rod-like particles with a prism body and pyramidal ends (samples HT8, HT24 and HT96 in Fig. 3, respectively). The particles are not yet uniformly shaped and some defects can be found on the surface. The average dimensions of the particles are around 80 nm in length and 30 nm in width, and they do not seem to change much during the time of the synthesis. An SAED pattern of the sample treated for 96 h (Fig. 3c) shows spots arranged in concentric circles, indicating that the rutile particles are considerably larger than those in the case of the commercial C2 sample. High-resolution TEM imaging reveals the presence of an amorphous layer, which is around 1 nm thick and uniformly covers the surfaces of the particles (Fig. 4).

3.2.2. FT-IR analysis

The results from the FT-IR spectroscopy are shown in Fig. 5. The samples prepared with the low-temperature technique (HT8, HT24, HT96 and C2) have a broad peak in the 3600–2800 cm^{-1} range, which can be attributed to the stretching vibrations of the interacting hydroxyl groups (Ti-OH) and the symmetric and antisymmetric vibrations of the molecular water coordinated to the Ti^{4+} ions [17]. The smaller band at 1630 cm^{-1} can be assigned to the bending vibrations of the same molecules. Both peaks stay the same after intensive drying at 110 °C for 24 h, which eliminates the possibility of physical water adsorption on the surface.

Table 1
Estimated crystallite sizes (Scherrer), specific surface areas and band-gap values of hydrothermally synthesized, high-temperature prepared and commercial phase-pure rutile samples.

Sample	Preparation conditions	Crystallite size (nm)	Specific surface area ($m^2\ g^{-1}$)	Band-gap (eV)
HT8	Hydrothermal synthesis (75 °C, 8 h)	13 ± 1	65 ± 5	3.06 ± 0.03
HT24	Hydrothermal synthesis (75 °C, 24 h)	14 ± 1	62 ± 5	3.11 ± 0.03
HT96	Hydrothermal synthesis (75 °C, 96 h)	13 ± 1	62 ± 5	3.07 ± 0.03
T800	Sol–gel synthesis, calcination (800 °C, 5 h)	50 ± 5	<2	2.97 ± 0.03
C1	No details	28 ± 4	7 ± 2	3.06 ± 0.03
C2	No details	8 ± 1	164 ± 6	3.10 ± 0.03

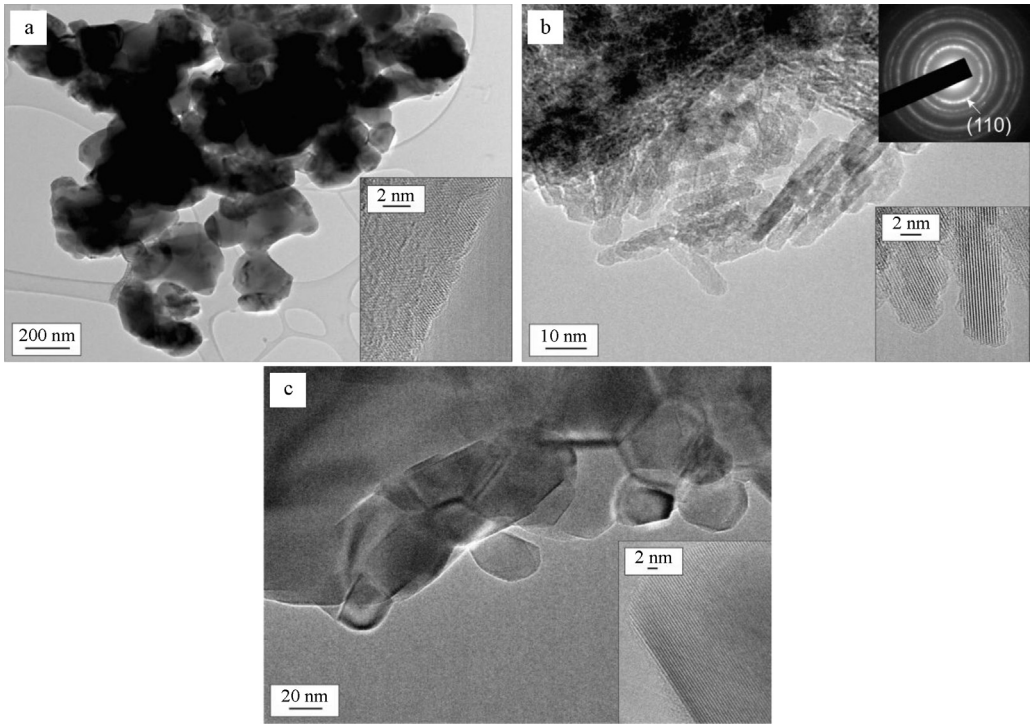

Fig. 2. TEM micrographs of the commercial rutile samples: (a) C1, (b) C2 and (c) T800 rutile TiO_2 crystals prepared with a high-temperature calcination at 800 °C (insets: HRTEM at higher magnification and SAED pattern (b)).

The samples synthesized with the high-temperature technique (C1, T800) have completely different FT-IR spectra: there are none of the characteristic peaks mentioned above, which indicates that high temperatures lead to the removal of the surface hydroxyl groups as well as the coordinated water molecules from the surfaces of the particles.

3.3. Photocatalytic activity

The results of the photocatalytic oxidation in the presence of oxygen gas after 1 h of reaction are shown in Fig. 6, together with the respective initial reaction rates (r_0) determined for all materials (namely, r_0 = 0.44, 0.37, 0.33, 0.25, 0.22 and 0.17 mg L^{-1} min^{-1}

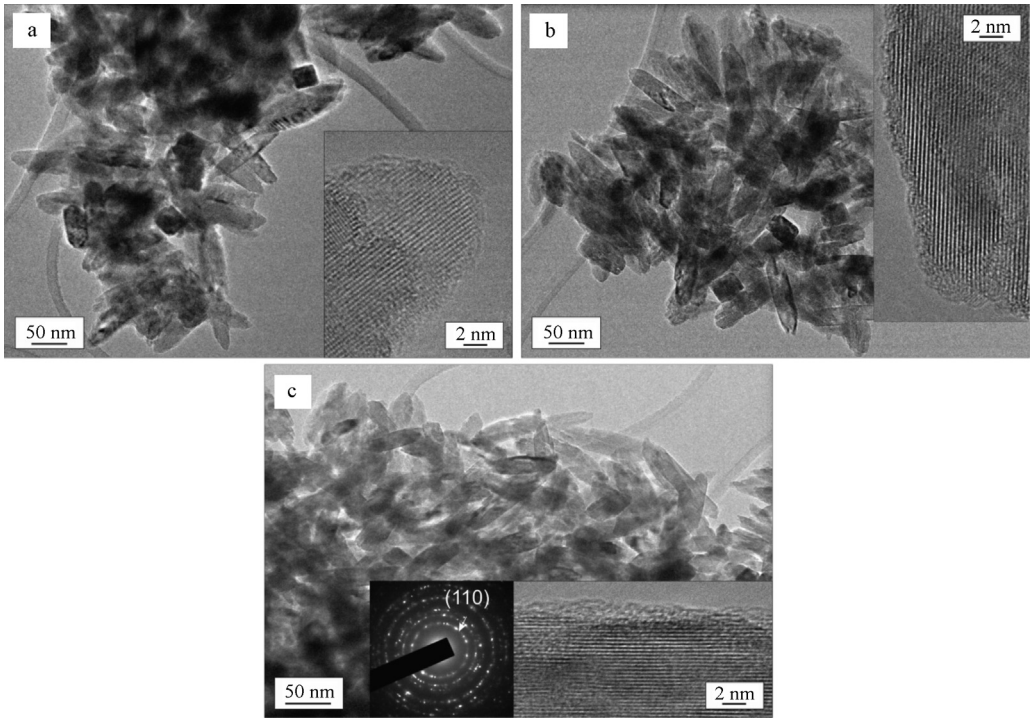

Fig. 3. TEM micrographs of rutile TiO_2 particles (nanorods) synthesized with hydrothermal treatment: (a) HT8, (b) HT24 and (c) HT96 (insets: HRTEM at higher magnification and SAED pattern (c)).

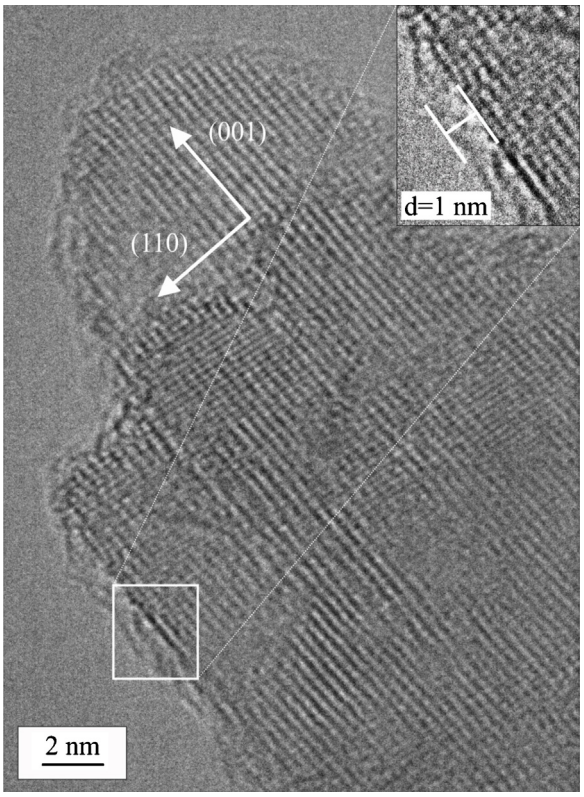

Fig. 4. High-resolution TEM image of rutile TiO_2 nanoparticle (HT8).

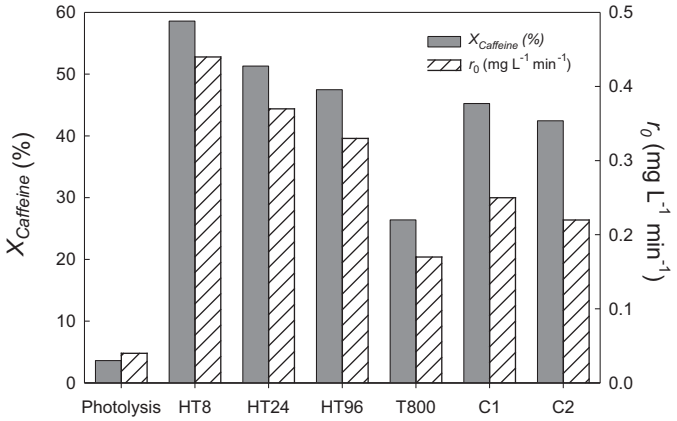

Fig. 6. Photocatalytic conversion (%) of caffeine after 1 h and initial reaction rate (r_0) with different TiO_2 samples in the presence of oxygen gas flow.

for HT8, HT24, HT96, C1, C2 and T800, respectively). It is clear that the sample synthesized with the low-temperature technique (HT8) exhibit the highest degradation rate: 60% of the caffeine was degraded in 1 h of reaction time ($r_0 = 0.44$ mg L^{-1} min^{-1}). The other two hydrothermally prepared samples (HT24 and HT96) show slightly lower photocatalytic activities ($r_0 = 0.37$ and 0.33, respectively), although they are still superior in comparison to the commercial rutile powders ($r_0 = 0.25$ and 0.22 mg L^{-1} min^{-1} for C1 and C2, respectively).

Surprisingly, the C2 sample oxidizes less caffeine than our samples and even less than the commercial C1 sample, although the specific surface area of C2 is much higher than all the other samples. It is commonly known that a high photocatalytic activity of titania particles can be obtained when two requirements are satisfied: a large surface area and a high crystallinity [18]. Particles from the C2 sample have a sufficient specific surface area, while the XRD spectra indicate the presence of an amorphous phase. Moreover, while the large, agglomerated particles of T800 sample oxidize less than 25% of the initial caffeine concentration in 1 h reaction time, the C1 sample with slightly larger specific surface area degrades

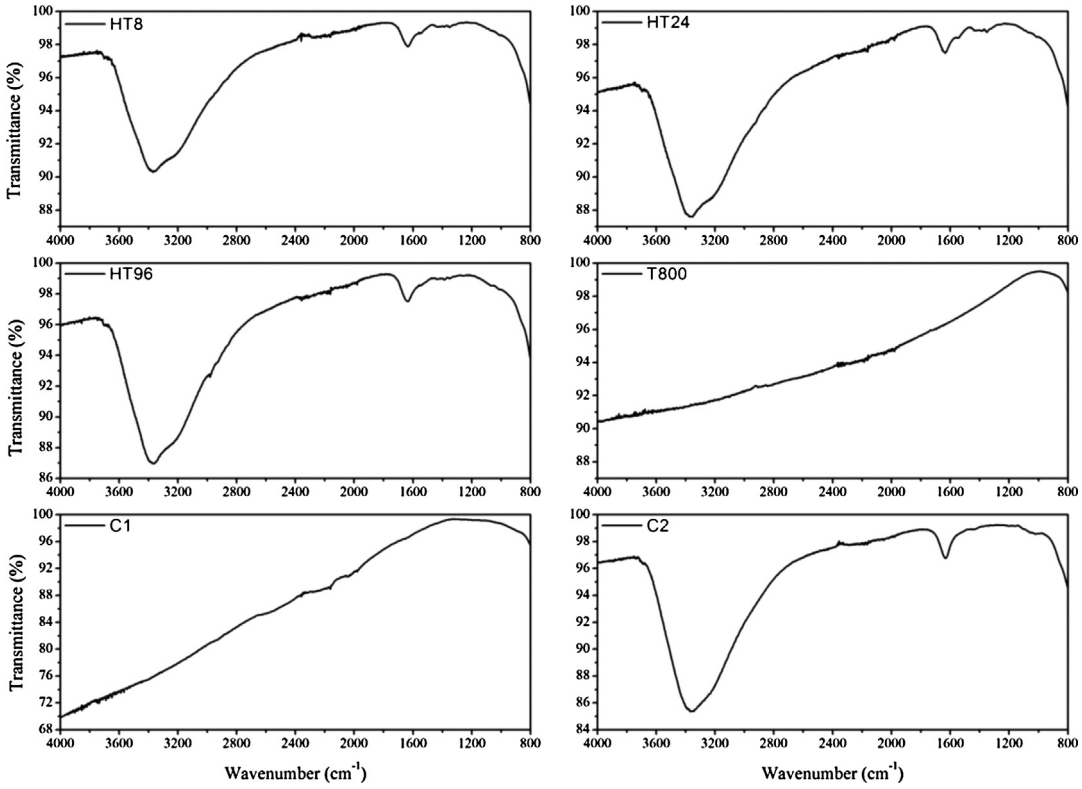

Fig. 5. FT-IR spectra of hydrothermally synthesized, high-temperature prepared and commercial phase-pure rutile samples.

almost twice as much. Obviously, the particle size is not the critical factor for efficient photocatalysis, therefore characterization of the surfaces is crucial for any understanding of the photocatalytic mechanism. In addition, the results of the photocatalytic activity in the presence of argon gas show no detectable activity (not shown), which reveals the importance of molecular oxygen as oxidation agent in the photocatalytic oxidation with rutile nanoparticles.

An experiment was also performed as reference in the presence of oxygen gas with the benchmark photocatalyst Degussa P25 which consists of both anatase and rutile crystalline phases of TiO_2. In this case the catalytic activity was significantly higher than for the samples prepared in the present work ($r_0 = 2.3\ mg\ L^{-1}\ min^{-1}$), probably due to the presence of the anatase crystalline phase.

3.4. Impact of surface properties on the photocatalytic activity

The observations of the particle surfaces with the HRTEM are consistent with the FT-IR results. The non-crystalline surface layer of the low-temperature samples can be assigned to the residual Ti^{4+} ions coordinated with water molecules and subsequently stabilized with the surface hydroxyl groups via hydrogen bonds. Surface hydroxyl groups in most cases act as binding sites for oxygen and polluting molecules and therefore increase the activity of the particles. As already mentioned, the high-temperature technique reduces the concentration of surface hydroxyl groups on the particles. The surface is flat, clean and the particles end with a crystal plane. In addition, the specific surface area (Table 1) generally decreases with an increase in the particle size.

Based on the photocatalytic results (Fig. 6), the first conclusion is that the particle size is not the limiting factor of this process. For instance, low-temperature hydrothermally treated samples have similar particle sizes but different photocatalytic activities, which could indicate that longer hydrothermal treatments may reduce the thickness of amorphous layer. Moreover, samples with larger (C1 and T800) or even smaller (C2) particles than low-temperature hydrothermally treated samples have lower activities.

Different gas-atmospheres (oxygen and argon flow, as well as natural air) gave us an insight into the surface function of the particles and led us to draw a tentative conclusion. When experiments were conducted without any gas flow, samples have almost identical activities as with the oxygen flow (differences in conversion lower than 5%), which suggests that the natural existing concentration of oxygen in the reaction medium is already sufficient enough for the photocatalytic process to occur. On the other hand, the experiments with argon gas show that argon molecules displace dissolved oxygen from the reaction medium, disabling the photocatalytic reaction with all samples since there is no electron carrier to collect the electrons from the conduction band and to prevent the immediate recombination. Therefore, it is not correct to assume that amorphous surface layer could be an effective electron trap, because no photocatalytic activity was observed in argon atmosphere when the samples were prepared by the low-temperature hydrothermal method.

The general mechanism of photo-induced semiconductor catalysis has been known for many years. The three main steps of the photodegradation mechanisms are: (i) reduction of oxygen molecules with the photoexcited electrons from the conduction band, resulting in reactive radicals which can oxidize the pollutant; (ii) oxidation of water molecules with the photogenerated holes from the valence band, the oxidation of the pollutant occurring with the respective reactive radicals that are formed; and (iii) direct oxidation of the pollutant with photogenerated holes. While these reactions are simultaneous, they take place on the surface of the particles; thus, the surface itself dictates the impact of each reaction mechanism on the photocatalytic efficiency. The surface of the hydrothermally treated particles is highly hydroxilated and hydrated and, therefore, dissolved oxygen molecules as well as pollutant molecules, which are present in the reaction mixture, can then adsorb on the functionalized surface faster and with higher affinity than on a flat surface. In fact, adsorbed oxygen molecules are an efficient consumer of electrons, which would otherwise accumulate in the conduction band and increase the recombination if their adsorption and consecutive reaction to form radicals is not fast enough [19,20]. Since the band-gap of rutile is lower than that of the anatase phase, the recombination becomes in this case the limiting factor in the oxidation reaction and, therefore, an efficient consumption of electrons is crucial in order to make the reaction effective.

Therefore, as expected, oxygen is the crucial molecule in the case of the photocatalytic degradation of caffeine molecule with rutile nanoparticles, and the functionalized surface seems to enhance the adsorption of dissolved oxygen molecules, or even the adsorption of the target pollutant in comparison to a flat surface, which results in an increased photocatalytic activity. This can justify why hydrothermally prepared samples showed the highest degradation rate in the presence of oxygen. Although these samples did not have the highest specific surface areas, the amorphous surface layer probably played the important role in the reactivity, absorbing the oxygen molecules on the surface of these samples faster and pro-longing the life-time of the photogenerated holes, which can participate in the degradation process by the formation of reactive radicals or by the direct oxidation of the pollutant. Caffeine adsorption in the dark was always lower than 4.0% of the initial caffeine concentration, but a higher adsorption of caffeine was generally observed on hydrothermally treated samples (as high as 3.9%) in comparison to the adsorption of caffeine when using the T800 (0.5%), C1 (1.5%) or C2 (1.8%) samples. Further experiments are being planned to follow the kinetics of the process and to confirm the mechanism.

4. Conclusions

The described two-step hydrothermal low-temperature synthesis leads to the formation of pure TiO_2 rutile phase, without the need of any additional thermal treatment. This synthetic route leads to the formation of rod-like shapes with a prism body and pyramidal ends, uniformly covered by a 1-nm-thick amorphous layer, containing surface OH groups and coordinated H_2O molecules.

The photocatalytic efficiency of these samples in the presence of oxygen gas is larger than the efficiency of the commercial (C1 and C2) and high-temperature (T800) samples and this is attributed to the presence of the amorphous surface layer.

Reactions in the absence of an oxidizing agent indicate that the amorphous surface layer observed in the materials prepared by a low-temperature hydrothermal method is not an effective electron trap on its own, because no photocatalytic activity was detected. However, the adsorption of dissolved oxygen, and caffeine, is more efficient in the functionalized surface that on a flat surface of rutile particles, because a higher photocatalytic activity was observed for hydrothermally treated samples.

As expected, molecular oxygen works as electron acceptor for the photoinduced electrons of the conduction band, while the caffeine degradation process is initiated in the photogenerated holes of the rutile particles, either by the formation of hydroxyl radicals, or via direct oxidation of the adsorbed caffeine molecule.

Acknowledgements

This work was performed under contract PR-03769 and Portugal-Slovenia Cooperation in Science and Technology and was supported by the Slovenian Research Agency within the program

P2-0084 and project J2-4309. The work is part of the Ph.D. thesis of Mr. Matic Krivec under Grant no. PR-03769. The financial support for this work was also partially provided by project PEst-C/EQB/LA0020/2011, financed by FEDER through COMPETE and by Fundação para a Ciência e a Tecnologia (FCT).

References

[1] M.R. Hoffmann, S.T. Martin, W. Choi, D.W. Bahnemann, Chemical Reviews 95 (1995) 69.
[2] A. Sclaffani, J.M. Herrmann, Journal of Physical Chemistry 100 (1996) 13655.
[3] A. Sclafani, L. Palmisano, M. Schiavello, Journal of Physical Chemistry 94 (1990) 829.
[4] J. Araña, J.M. Doña-Rodríguez, D. Portillo-Carrizo, C. Fernández-Rodríguez, J. Pérez-Peña, O. González Díaz, J.A. Navío, M. Macías, Applied Catalysis B: Environmental 100 (2010) 346.
[5] A. Fujishima, X. Zhang, D.A. Tryk, Surface Science Reports 63 (2008) 515.
[6] S. Liu, N. Jaffrezic, C. Guillard, Applied Surface Science 255 (2008) 2704.
[7] Z. Zhang, C.-C. Wang, R. Zakaria, J.Y. Ying, Journal of Physical Chemistry B 102 (1998) 10871.
[8] Y.-F. Chen, C.-Y. Lee, M.-Y. Yeng, H.-T. Chiu, Journal of Crystal Growth 247 (2003) 363.
[9] Y. Zhang, L. Wu, Q. Zeng, J. Zhi, Journal of Physical Chemistry C 112 (2008) 16457.
[10] L.-C. Chuang, C.-H. Luo, S.-W. Huang, Y.-C. Wu, Y.-C. Huang, Advances in Materials Research 214 (2011) 97.
[11] S. Sauvé, K. Aboulfadl, S. Dorner, P. Payment, G. Deschamps, M. Prévost, Chemosphere 86 (2012) 118.
[12] M.J. Sampaio, C.G. Silva, R.R.N. Marques, A.M.T. Silva, J.L. Faria, Catalysis Today 161 (2011) 91.
[13] K. Tomita, V. Petrykin, M. Kobayashi, M. Shiro, M. Yoshimura, M. Kakihana, Angewandte Chemie International Edition 45 (2006) 2378.
[14] B. Qi, L. Wu, Y. Zhang, Q. Zeng, J. Zhi, Journal of Colloid and Interface Science 345 (2010) 181.
[15] M. Nag, D. Guin, P. Basak, S.V. Manorama, Materials Research Bulletin 43 (2008) 3270.
[16] H.-S. Lee, C.-S. Woo, B.-K. Youn, S.-Y. Kim, S.-T. Oh, Y.-E. Sung, H.-I. Lee, Topics in Catalysis 35 (2005) 255.
[17] A.J. Maira, J.M. Coronado, V. Augugliaro, K.L. Yeung, J.C. Conesa, J. Soria, Journal of Catalysis 202 (2001) 413.
[18] M. Kaneko, I. Okura, Photocatalysis: Science and Technology, Kodansha-Springer, Lexington, 2010.
[19] M. Tasbihi, C.R. Ngah, N. Aziz, A. Mansor, A.Z. Abdullah, L.K. Teong, A.R. Mohamed, Industrial and Engineering Chemistry Research 46 (2007) 9006.
[20] R. Al-Rasheed, D.J. Cardin, Chemosphere 51 (2003) 925.